



Uncertainty analysis of SPI and SRI calculation using bootstrap in the Mediterranean regions of Algeria

Mohammad Achite^{1,2} · Ommolbanin Bazrafshan³  · Zohreh Pakdaman⁴ · Andrzej Wałęga⁵ · Fateme Pourhaghverdi³ · Tommaso Caloiero⁶

Received: 24 September 2023 / Accepted: 20 April 2024
© The Author(s), under exclusive licence to Springer Nature B.V. 2024

Abstract

The standardized precipitation index (SPI) and the standardized runoff index (SRI) are widely used in drought monitoring. In the calculation of these indices, the time scale and distribution functions are especially significant. In the current study, the uncertainty in the estimation of the two indices, in terms of time scale and distribution functions, was investigated in the wadi Mina basin (Algeria) using monthly precipitation and runoff values based on the gamma-II (GAM-II), extreme value-III (EVD-III), Pierson-III (PEI-III) and Weibull-II (WEI-II) distribution functions. With this aim, precipitation and runoff amounts were calculated considering 12- and a 24-month time scales; then, using the bootstrap method, 1000 random sample were generated for each precipitation and runoff event and for each time scale, and the confidence interval of the two indices was calculated at around 95%. The size of the confidence interval was considered as uncertainty and the error rate between the estimated and observed data was calculated. The results showed that all the considered distributions fit the time series acceptably, and that the time scale of the data is not significantly correlated with the goodness of fit. Moreover, there is no apparent relationship between the rejection cases and the scale and position of the regional stations or the investigated variables. The lack of significant differences between the observed and estimated time series for a specific distribution caused the averages estimated in SPI to fall within the same descriptive class. Based on the results, WEI-II and EVD-III showed the lowest estimation error and uncertainty in meteorological and hydrological drought, respectively, at both 12- and 24-month time scales, thus suggesting the use of these two functions for drought monitoring at medium-term and long-term time scales.

Keywords Drought monitoring · Uncertainty · Bootstrap · Sampling · Precipitation index · Standardized runoff

1 Introduction

Territories overlooking the Mediterranean basin, considered a highly vulnerable area to climate change, are particularly susceptible to the adverse effects of drought due to its irregular precipitation patterns (Tramblay et al. 2020). As an example, in recent years North

African regions have witnessed an increase in the frequency and severity of drought events, leading to growing concerns regarding water scarcity, food security, and ecosystem health (Spinoni et al. 2014).

Meteorological and hydrological droughts are complex phenomena driven by a combination of climatic and hydrological factors. Meteorological droughts are primarily characterized by a prolonged deficit in precipitation, while hydrological droughts manifest as decreased streamflow, groundwater levels, and reservoir storage, impacting water availability in various sectors (Achite et al. 2023). Generally, drought indices are a widely adopted tool for the evaluation of drought conditions. Among the various indices one of the most applied is the standardized precipitation index (SPI) that was initially formulated by McKee et al. (1993). The SPI operates on the basic principle of converting the probability of cumulative precipitation on different time scales into an index. This flexible approach allows the assessment of different types of droughts: shorter time scales are suitable for meteorological and agricultural drought assessments, while longer time scales prove more suitable for characterizing hydrological and water resource-related droughts. This index serves multiple purposes, acting as a valuable tool for assessing drought severity, issuing early warnings about droughts, and discerning the influence of climate change, as several studies highlighted, e.g. Bordi et al. (2009), Buttafuoco and Caloiero (2014), and Buttafuoco et al. (2018). In addition, the SPI boasts several advantageous features. First, it is based solely on precipitation data, making it possible to assess drought even in the absence of other hydrometeorological measurements. Second, its adaptability to different time scales makes it possible to evaluate drought conditions in different meteorological, hydrological and agricultural contexts. Finally, the standardization of the SPI ensures that the frequency of extreme drought events remains relatively constant across locations and time scales, as demonstrated by Lloyd-Hughes and Saunders (2002) and Hayes et al. (1999). Consequently, it maintains its status as a robust and widely favored index for meteorological drought diagnosis, making it the preferred choice for researchers to unravel and characterize drought events in terms of duration and intensity (Bordi et al. 2004). Alongside its advantages, the potential disadvantages associated with the SPI should be considered. These include the difficulty of finding appropriate probability distribution functions to model observed precipitation patterns, as highlighted by Guttman (1999), Wu et al. (2007), and Angelidis et al. (2012). Another disadvantage in the use of the SPI is that sufficiently lengthy time series data are necessary to ensure dependable estimates, as emphasized by Guttman (1994, 1999) and Wu et al. (2005). In addition, the potential inability to identify the onset of drought (Wu et al. 2007) or its conclusion (Blain 2012) should be considered in cases where SPI series deviate from normal distributions, often seen in precipitation data with a high frequency of zero values. Finally, the omission of other climate variables, such as temperature which, as underscored by Vicente-Serrano et al. (2010), may be crucial in the context of climate warming, because this variable makes it possible to include precipitation loss, like evaporation, in the drought analysis. Nevertheless, given the importance of the SPI, Shukla and Wood (2008) applied the concept employed by McKee et al. (1993) for the SPI in defining the standardized runoff index (SRI) as the unit standard normal deviate associated with the percentile of accumulated hydrologic runoff over a specific duration.

As previously evidenced, the identification of a probability distribution suitable to describe precipitation or runoff data can be considered a possible source of uncertainty in the SPI or SRI evaluation. In effect as underlined by Guttman (1999), if different distributions are used to describe an observed series of precipitation or runoff data, as a result, different SPI or SRI values may be obtained. Accurate assessment and

quantification of the uncertainties associated with drought indices and their impacts are crucial for effective drought management and mitigation strategies. For this reason, some authors have conducted analyses to examine the impact of probability distribution selection and record length on the calculation of drought indices or the evaluation and comparison of all sources of uncertainty inherent in drought index estimates. For example, recent studies (Naumann et al. 2012; Hu et al. 2015) have introduced bootstrap-based methods to quantify the uncertainty associated with the SPI calculations. Specifically, in the work of Naumann et al. (2012), the primary focus was to compare the SPI confidence intervals derived from datasets of varying lengths, while Hu et al. (2015) predominantly discussed the impact of sampling uncertainty on the estimation of SPI value. Vergni et al. (2018) employed a bootstrap-based approach to evaluate how the SPI confidence intervals behave when subjected to variations in multiple sources of uncertainty: the underlying probability distribution, time scale, time series length, and month (for time scales shorter than 12 months). Ghasemnezhad et al. (2022) analyzed the uncertainty of the SRI in Iran for different time scales, from 3 to 48 months, using the Monte Carlo sampling and considering normal, log normal, Weibull and gamma distribution functions. The results showed that the highest uncertainty is related to the normal and log normal distributions and the lowest uncertainty is related to the gamma and Weibull distributions. In addition, increasing the time scale and decreasing the length of the record led to an increase in uncertainty.

In this context, the objective of this scientific paper is to enhance our understanding of meteorological and hydrological droughts in a Mediterranean area (Algeria) by conducting a rigorous uncertainty analysis using the Bootstrap resampling technique. The findings of this research may offer valuable insights into drought monitoring, early warning systems, and water resource management practices in this climatically vulnerable region, ultimately fostering the development of more resilient and sustainable strategies for addressing drought challenges.

1.1 Study area and data collected

The study area is the Wadi Mina basin, in northwest of Algeria, which covers an area of 4900 km² and lies between 00° 22' 59" E and 01° 09' 02" E and between 34°41'57" N and 35° 35' 27" N (Fig. 1). The wadi Mina involves four major tributaries: wadi Mina, wadi Haddad, wadi Abd and wadi Taht. The topography of the basin is complex and rugged, and the altitude varies from 164 to 1327 m. The climate at the study area is continental with cold winters and hot summers with large temperature differences. Average annual precipitation in the basin ranges from 250 to 500 mm, mostly concentrated between November and March, while the mean annual temperature ranges from about 16–19.5 °C. Almost half of the basin is covered by vegetation of varying densities, such as scrubs (32%), forests (35.8%), and cereal crops (Achite and Ouillon 2007). Monthly precipitation and runoff records for a 40-year observation period (1974–2009) were compiled for five precipitation (S1, S2, ..., S5) and hydrometrics (H1, H2, ..., H5) stations from the National Agency of the Water Resources (Fig. 1 and Tables 1 and 2). Data were examined for homogeneity using the double mass curve, linear regression, and Mann–Whitney test procedures to ensure quality. The technique found a few in homogeneities, and the irregular data were corrected using data from nearby homogeneous stations (Achite et al. 2021).

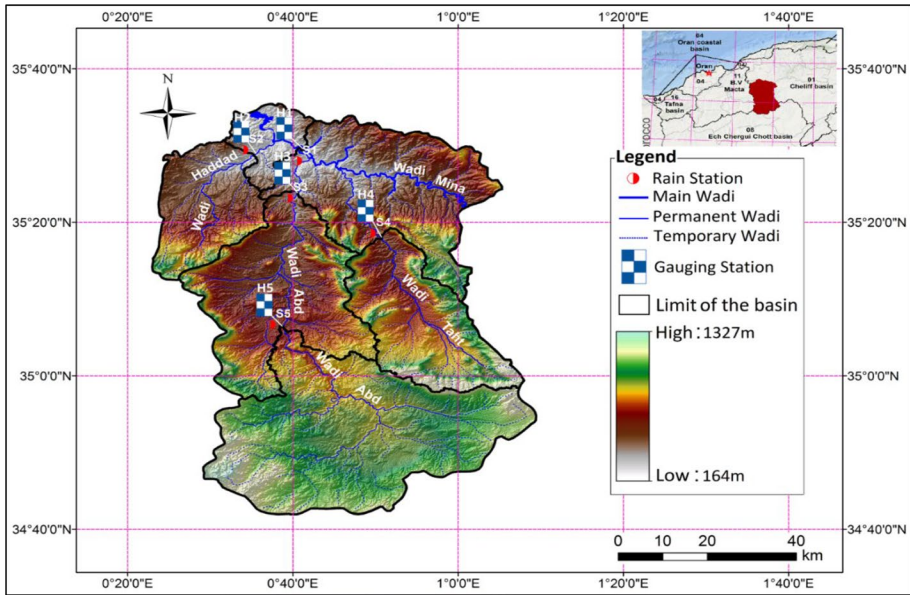


Fig. 1 Map of the study area along with located hydro-meteorological stations

Table 1 Precipitation stations characteristics

ID	Code	Name	Longitude	Latitude	Elevation (m)	Mean	STDEV
S1	013306	Oued Abtal	0° 40' 33.97" E	35° 28' 03.59" N	354	21.57	21.73
S2	013401	Sidi Abdelkader Djillali	0° 34' 08.35" E	35° 29' 20.71" N	225	20.11	21.30
S3	013302	Ain Hammara	0° 39' 16.85" E	35° 23' 15.39" N	288	21.13	21.93
S4	013001	Kef Mehboula	0° 49' 34.20" E	35° 18' 40.72" N	475	27.29	27.10
S5	013304	Takhmaret	0° 37' 27.25" E	35° 06' 49.01" N	655	20.63	21.21

2 Methodology

2.1 Standardized precipitation index (SPI) and standardized runoff index (SRI)

The calculation process for the SPI and the SRI is exactly the same but with precipitation data as input for SPI and runoff data as input for SRI (Bazrafshan et al. 2015). The process starts with fitting the appropriate probability distribution function to the data series in any desired time interval. If X represents the total amount of the variable during a period of τ month in month j , by fitting the desired distribution to the time series of X , the density distribution function or marginal CDF $u = F_{X\tau(x\tau)}$ is obtained. Then the index is calculated for each observation with the inverse normal function or $\Phi^{-1} = (u_\tau)$. In other words, instead of showing cumulative probability, the index is described by a standard normal variable (with zero mean and 1 standard deviation).

Table 3 shows the classification of drought severity based on SPI or SRI values.

Table 2 Gauging stations characteristics

ID	Code	Name	Basin area (km ²)	Longitude	Latitude	Elevation (m)	Mean	STDEV
SH1	013402	Oued Abtal	4126	0°41'00.49" E	35°29'26.28" N	210	1.90	2.71
SH2	013402	Sidi Abdelkader Djillali	480	0°35'19.99" E	35°28'46.05" N	241	0.16	0.33
SH3	013302	Ain Hammara	2480	0°40'33.19" E	35°23'50.09" N	285	1.17	1.85
SH4	013001	Kef Mehboula	680	0°50'47.89" E	35°18'05.21" N	502	0.32	0.56
SH5	013301	Takhmaret	1553	0°38'46.54" E	35°06'20.08" N	634	0.73	1.81

Table 3 SPI/SRI drought severity classification (McKee et al. (1993))

Drought severity classes	Threshold value	Abbreviations
Extreme wet	> 2	ED
Severe wet	1.5–2	SW
Moderate wet	1–1.5	MOW
Mild wet	0.5–1	MIW
Normal	0.5–(–0.5)	N
Mild drought	– 1–– 0.5	MID
Moderate drought	– 1–– 1.5	MOD
Severe drought	– 1.5–– 2	SD
Extreme drought	< – 2	ED

2.2 Drought characteristics

The drought characteristics investigated this study are duration, severity, magnitude and peak. According to McKee et al. (1993), a drought event is defined as a period in which the SPI or the SRI values are less than zero. Consequently, the drought duration (D) refers to the period during which drought values consistently remain below zero, and the accumulated drought values within each event represent the drought severity (S), which for convenience is considered as an absolute value as follows:

$$S = \left| \sum_{i=1}^D SPI_i \right| \quad (1)$$

The drought magnitude results from dividing the severity by the duration within each event (Azhdari et al. 2021). Finally, the drought peak is the maximum value of S in a period of D months.

2.3 Resampling using bootstrap method

This method is classified in the group of non-parametric statistics methods and resampling techniques and is used to estimate the parameter of a statistical population using sampling with placement. Bootstrap is also used to calculate the confidence interval for the estimation (Verdonck et al. 2001). In the bootstrap method, subsamples are generated by resampling with replacement from the original sample. Considering that the number of original samples is equal to n , it is possible to create infinite sub-samples of size n with placement (Dixon 2006).

The bootstrap steps in this research are as follows:

Step 1: N times from the main precipitation or runoff data values $X = X_1 \dots X_n$ should be sampled by the sampling method with placement, then N groups resulting from the bootstrap samples will be obtained.

$$X_{(j)}^* = X_{1(j)}^* \dots X_{n(j)}^* \text{ for } j = 1 \dots N \quad (2)$$

Step 2: Using the maximum likelihood method, the theta parameter of the distribution function $f(x,\theta)$ based on each bootstrap sample $X_{(j)}^*, j = 1 \dots N$ is estimated. Then N sets of $\theta_{(j)}^*, j = 1 \dots N$ parameters are obtained.

Steps 3: For a given precipitation or runoff event $X_{i,i} = 1 \dots n$ using eqs. 3 and 4 and using N sets of parameters $\theta_{(j)}^*$, the number N estimate the cumulative probability $H(x_i)$ as $H(X_{i,(j)}), i = 1 \dots n; j = 1 \dots N$ can be calculated.

$$SPI(orSRI) = \theta^{-1}(F(X)) \tag{3}$$

$$H(x) = q + (1 - q)F(x) \tag{4}$$

Step 4: Using Eq. 5, the SPI or the SRI value is estimated for events $X_{i,i} = 1 \dots n$ according to estimates of the cumulative distribution function that values $H(X_{i,(j)}), i = 1 \dots n; j = 1 \dots N$; then to calculate the SPI or SRI for each phenomenon x_i , N estimates of SPI or SRI are obtained as $SPI(orSRI)_{i,(j)}$ for $i = 1 \dots n; j = 1 \dots N$.

$$SPI(orSRI) = \theta^{-1}(H(X)) \tag{5}$$

Step 5: By putting the $SPI(orSRI)_{i,(j)}$ values for $i = 1 \dots n; j = 1 \dots N$ as the sampled SPI or SRI for the data event x_i , based on it, a point estimate or an interval estimate for SPI or SRI can be obtained (Hu et al. 2015).

2.4 SPI and SRI bootstrap sampling algorithm

To evaluate SPI or SRI, the first step was to calculate the amount of cumulative precipitation or runoff in the year i and the month j , which ranges from 1 to 12. The value of j depends on the time scale τ , which can be any scale from 1 to 48 months.

$$Y_{i,j}^\tau = \sum_{t=0}^{\tau-1} X_{i,j-t} \tag{6}$$

where x_{ij} is the amount of monthly precipitation or runoff for the year i and the month $j = 1.2 \dots .12$ and; $Y_{i,j}^\tau$ is the cumulative precipitation or runoff value for the desired τ scale.

As an example, $Y_{1983,12}^{12}$ means the scale of one month, in the twelfth month (December) 1983 ($\tau = 12; j = 12$ and $i = 1983$).

In current study, we applied the Gamma (GA), Weibull (WEI), Extreme value (EVD) and Pearson (PE) distributions (Fig. 2).

Based on the presented method to calculate the uncertainty, starting from precipitation or runoff data for $Y_{i,12}^{12}$, which means 1 month scale in the 12th month of 1974–2009, resampling has been done 1000 times with bootstrap as follows:

$$Y_{i,12(j)}^{*12} = \left(y_{1974.9(j)}^{*12} \cdot y_{1975.12(j)}^{*12} \cdot y_{1976.12(j)}^{*12} \cdot \dots \dots \dots y_{2009.12(j)}^{*12} \right) for j = 1, 2, \dots \dots \dots, 1000 \tag{7}$$

In the next step, based on each bootstrap sample, $Y_{i,12(j)}^{*12}$ a set of 1000 parameters of θ_j^* of each function has been obtained. Then, using relations Eqs. 1, 2 and 3, there are 1000 estimates of SPI or SRI according to the amount of precipitation or runoff from $Y_{i,12}^{12}$, for which $SPI(orSRI)_{i,j} = 1 \dots 1000$ can be obtained. Finally, from these thousand estimates, it is possible to calculate the upper and lower bounds based on the 5% and 95% quantile.

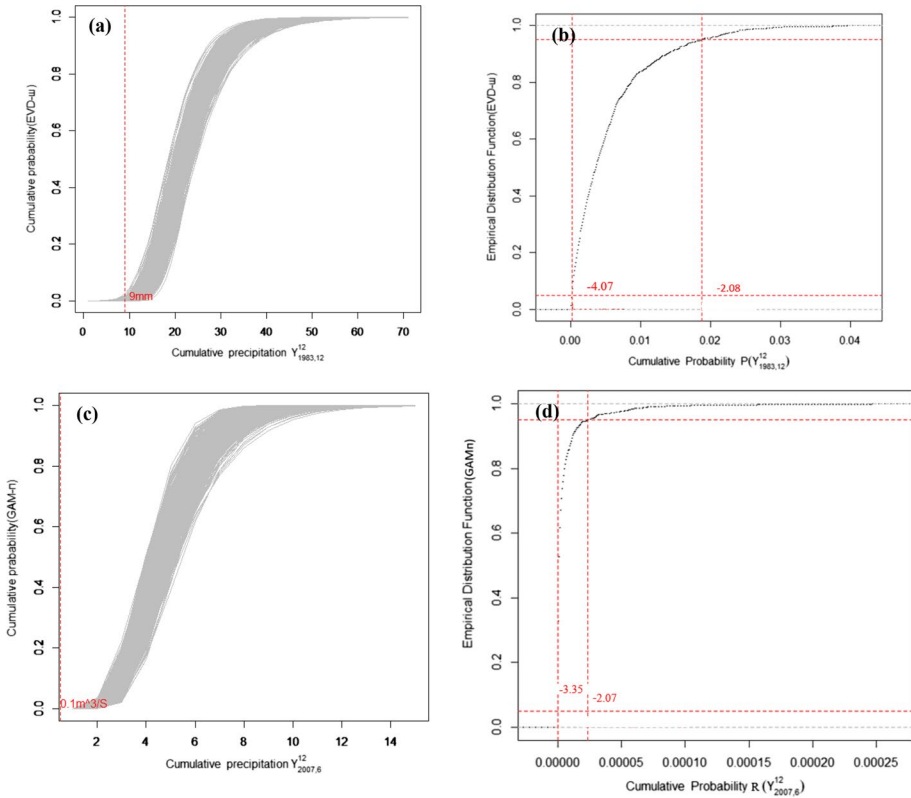


Fig. 2 The interval for SPI and SRI, by bootstrap method procedure. For example, for SPI, $\tau = 12$; $j = 12$ and $i = 1983$ precipitation is 9 mm. (a) The M ($M = 1000$) EVD cumulative distribution functions (fitted to each sample bootstrap from the original precipitation data), and M possible values of cumulative probability $P(X_{1983,12}^{\tau})$ are estimated, (b) the empirical cumulative distribution function of the M values of $P(X_{i,j}^{\tau})$, and the 0.5th $P(X_{i,j}^{\tau}) = 0.0001$ and 0.95th $P(X_{i,j}^{\tau}) = 0.018$ percentile discovered. The lower and upper limits of the SPI confidence ($P = 90\%$) is -4.07 and -2.08 respectively; (c, d) repeated for SRI

2.5 Estimation of error

Equation 8 was used to compare the efficiency of the bootstrap simulation values with the observed values as suggested by Hugh et al. (2015).

$$ARE = \left| \frac{(SPI_{Obs} - SPI_{Est})}{SPI_{Obs}} \right| \times 100 \tag{8}$$

in which ARE is the absolute value of the error ratio and SPI_{Obs} and SPI_{Est} are the observed value and the average value of the estimates in 1000 times of sampling in each time scale, respectively.

2.6 Kappa Kohen weighted (Kw)

In order to compare the observed and predicted classes of SPI and SRI, the Cohen’s kappa statistic was used. Kappa statistic was first introduced by Cohen (1968) as a measure of agreement in psychology. Given that P_{ij} is the ratio of the total components of the time series that belong to class i of one series and to class j of the second series, these ratios can be formed inside a matrix whose main diameter contains the unique P_{ii} ratios of the components that match in both series and P_o is the sum of P_{ii} values. Considering $P_{e,ii}$ as the product of the sum of the respective row and column ratios ($P_{e,ii}=P_{oi} \cdot P_{i\bullet}$), the expected agreement value is equal to the sum P_e of the $P_{e,ii}$ values. The Kappa statistic is then defined as:

$$K = \frac{P_o - P_e}{1 - P_e} \tag{9}$$

Landis and Koch (1977) presented Table 4 to classify agreement into different categories. In the comparison of SPI or SRI classes in the observed and predicted series, the disagreement between mild drought and moderate drought is not as big as the disagreement between mild drought and severe drought. Therefore, by considering specific weights for each of the non-agreement states, a more accurate comparison of the SPI or SRI classes in the observed and predicted series can be made. By considering the weighted w_{ij} for the disagreement in the ij domain of the matrix, the weighted disagreement is obtained from the sum of the products of the ratio $P_{ij} \times w_{ij}$. Therefore, the weighted kappa statistic is obtained from the following equation:

$$K = 1 - \frac{\sum w_{ij} P_{ij}}{\sum w_{ij} P_{e,ij}} \tag{10}$$

The significance test statistic of the weighted kappa statistic with the null hypothesis of disagreement is as follows:

$$t = \frac{K}{\sqrt{\frac{\sum w_{ij}^2 P_{e,ij} - (\sum w_{ij} P_{e,ij})^2}{n(\sum w_{ij} P_{e,ij})^2}}} \tag{11}$$

where n is the number of time series observations.

Table 4 Description of Kw and value of agreement

Kw statistics	Agreement
<0.00	Poor
0.00–0.20	Slight
0.21–0.4	Fair
0.41–0.6	Moderate
0.61–0.8	Substantial
0.81–1	Almost perfect

3 Results and discussion

3.1 Goodness of fit

The evaluation of the efficiency of the four mentioned functions and the goodness-of-fit test on precipitation and runoff data in the five climatological and hydrological stations are shown in Table 5, which provides K–S and *P*-value statistics for each distribution.

Rejection percentages are similar among the distributions, with GAM-II and EVD-III performing slightly better (no rejection) than PE-III and WEI-II (5% rejection). Therefore, in general, the performance of all four candidate distribution functions can be considered acceptable. The noteworthy point is that the goodness-of-fit test is not significantly related to the time scale, so that 5% rejection occurred in both 12 and 24 month scales. Furthermore, no apparent relationship has emerged between the rejection cases with the scale and position of the regional stations or the investigated variable. The results of Vergni et al. (2017), Stagge et al. (2015), Lloyd-Hughes and Saunders (2002) and Khatun et al. (2007), Bazrafshan et al. (2020) also reported the same results on goodness of fit.

Table 5 Kolmogorov–Smirnov test for precipitation and runoff

Variable	St.name	Time scale	PE-III		GAM-II		GEV-III		WEI-II	
			K-S	<i>P</i> _{value}	K-S	<i>P</i> _{value}	K-S	<i>P</i> _{value}	K-S	<i>P</i> _{value}
Precipitation	S1	12	0.02	0.41	0.03	0.14	0.02	0.41	0.05	0.6
		24	0.025	0.51	0.028	0.39	0.02	0.64	0.05	0.3
	S2	12	0.02	0.73	0.01	0.91	0.02	0.76	0.02	0.48
		24	0.030	0.30	0.024	0.61	0.025	0.50	0.02	0.81
	S3	12	0.03	0.29	0.020	0.79	0.029	0.33	0.021	0.75
		24	0.01	0.95	0.04	0.76	0.02	0.51	0.03	0.23
	S4	12	0.024	0.55	0.033	0.22	0.02	0.71	0.021	0.76
		24	0.02	0.77	0.02	0.80	0.03	0.10	0.02	0.40
	S5	12	0.020	0.80	0.01	0.96	0.04	0.022	0.04	0.06
		24	0.01	0.83	0.03	0.24	0.02	0.62	0.02	0.46
Runoff	SH1	12	0.023	0.65	0.023	0.63	0.01	0.92	0.026	0.48
		24	0.029	0.34	0.015	0.97	0.33	0.204	0.026	0.50
	SH2	12	0.024	0.60	0.024	0.59	0.020	0.78	0.04	0.042
		24	0.018	0.88	0.031	0.26	0.027	0.45	0.021	0.75
	SH3	12	0.021	0.761	0.02	0.49	0.024	0.58	0.02	0.56
		24	0.03	0.23	0.034	0.18	0.03	0.32	0.047	0.22
	SH4	12	0.032	0.23	0.017	0.91	0.03	0.22	0.03	0.26
		24	0.024	0.359	0.030	0.30	0.02	0.54	0.018	0.89
	SH5	12	0.03	0.23	0.022	0.71	0.02	0.76	0.032	0.25
		24	0.04	0.01	0.02	0.34	0.03	0.25	0.017	0.92
Percentage of rejection at 5% significant level		5%		5%		0%		0%		5%

Bold number: No significant at 95%level

Table 6 shows the descriptive statistics including mean, minimum, maximum and standard deviation of SPI and SRI at the 95% confidence level for the 12- and 24-month time scales and the investigated stations considering the four investigated functions.

Based on the results, the averages estimated in SPI are in the same descriptive class, so that the extreme meteorological wet (maximum SPI) is estimated by the PE-III function and the extreme meteorological drought (minimum SPI) is estimated by the EVD-III function, which has the highest standard deviation. In hydrological drought, the most severe hydrological drought is estimated by WEI-II, but the most severe hydrological drought and the highest standard deviation is estimated by GAM-II, which is often seen in a 12-month time scale.

3.2 Election of distribution function and time scale on drought monitoring

SPI and SRI were extracted in the 12- and 24-month time scales with four distribution functions, and drought events were estimated based on the classification proposed by McKee et al. (1993). Figure 3 (a, b) shows the SPI and Fig. 3 (c, d) the calculated SRI at station S1 and SH1 for the 12- and 24-month time scales. The SPI on a 12-month scale has several fluctuations, so that the duration of drought changes with different intensity and weakness in different years. Several historical wet/dry events have been detected by all functions for the SPI and the SRI at both 12- and 24-month time scales (Table 7). For example, on a 12-month scale ($\tau = 12$), in 1983 ($i = 1983$) in December ($j = 12$), with 9 mm of precipitation, the most severe drought ($SPI = -3.72$) has been estimated by the EVD-III, followed by the GAM-II ($SPI = -3$), while the WEI-II and the PE-III estimated -2.06 and -2.05 respectively. Considering the event $Y_{1975,6}^{12}$ with $P = 39$ mm, the WEI-III has estimated the most severe wet period ($SPI = -3.10$) followed by the PE-III ($SPI = -2.81$), the GAM-II ($SPI = -2.67$) and the EVD-III ($SPI = -2.23$). Considering the 24-month scale, two short-term drought periods and two long-term drought periods have been observed, in which the historical drought event $Y_{2000,5}^{24}$ occurred. Similar to the 12-month scale, the EVD-III has estimated the most severe drought ($SPI = -3.14$) followed by the WEI-II ($SPI = -1.53$). In general, for the meteorological drought, EVD-III estimated the most severe drought while the WEI-II has estimated the values of lower intensities.

Regarding hydrological wet and drought events, the SRI showed three long-term drought periods for the 12-month time scale and, in the period 2003–2007, two historical events $Y_{2005,8}^{12}$ and $Y_{2007,6}^{12}$ occurred. On a scale of 24 months, the duration of drought is increasing and a historical event $Y_{2005,12}^{24}$ occurred. The GAM-III estimated the most severe droughts in all the years while the PE-III showed the least severity of drought. On the other hand, considering the historical wet events $Y_{1981,5}^{12}$, $Y_{1998,5}^{12}$ and $Y_{1975,12}^{24}$ were rated as the most severe for the PE-III while the EVD-III evidenced the least severity.

Figure 4 shows the drought zoning in two historical events of meteorological (Fig. 4a) and hydrological (Fig. 4b) drought with the help of the EVD-III and the GAM II functions, respectively, in Mina basin. The above occurrences are the most exceptional droughts that have been mentioned by the functions during the study period. In the event $SPI_{1983,12}^{12}$ the most vulnerable parts of the region in terms of lack of precipitation have been identified in the southern parts, while in event $SRI_{2007,6}^{12}$ the most vulnerable points in terms of surface currents have been detected in the northern regions.

Figure 5 is calculated considering the classification (9 categories) proposed by Lloyd-Hughes and Saunders (2002) for two time scales and two indicators investigated in stations S1 and SH1. Based on the results of the SPI-12 (Fig. 5a), most of the frequency of

Table 6 Descriptive statistics of the SPIASRI at 95%confidence interval

Variable	St. name	Time scale	Mean PE-III	Max	Min	STDEV	Mean GAM-II	Max	Min	STDEV
Precipitation	S1	12	0.07	2.87	-2	0.991	-0.000	2.72	-3.001	0.999
	S2	24	0.11	3.04	-1.7	0.992	-0.000	3.15	-2.28	0.999
		12	0.04	2.7	-2.2	0.994	-0.000	2.65	-3.37	1
	S2	24	-0.09	2.77	-2.1	0.993	-0.003	2.41	-2.14	0.999
		12	0.01	3.46	-2.4	0.996	-0.000	3.41	-3.65	0.999
Runoff	S4	24	0.1	2.97	-1.6	0.992	-0.000	3.2	-1.99	0.999
		12	0.005	3.08	-2.4	0.995	-0.000	2.59	-3.36	0.999
	S5	24	-0.02	3.18	-2	0.997	-0.000	2.58	-2.31	1
		12	0.02	2.86	-2.7	1	-0.000	2.6	-4.29	1
	SH1	24	-0.004	2.94	-2.5	0.99	-0.000	2.53	-2.87	0.999
SH1		12	-0.006	3.5	-2.2	1	0.009	1.69	-3.05	1
		24	-0.01	3.001	-2.5	0.94	0.003	1.62	-2.49	1
SH2		12	0.05	3.83	-1.1	0.995	0.009	2.38	-2.62	1
		24	-0.03	2.95	-1.4	1	0.008	1.83	-2.49	1
SH3	SH3	12	-0.1	3.61	-1.6	0.996	-0.000	2.44	-2.007	0.999
		24	-0.05	3.12	-2	0.997	0.000	2.32	-2.37	1
	SH4	12	0.23	3.26	-1.3	0.968	0.08	3.67	-2.7	1.21
		24	0.08	3.35	-1.4	0.992	-0.000	3.9	-2.24	0.999
	SH5	12	0.51	2.66	-0.78	0.857	-0.02	3.35	-1.72	0.99
24		0.48	2.35	-0.7	0.879	-0.01	2.5	-1.57	0.995	

Table 6 (continued)

Variable	St.name	Time scale	Mean GEV-III	Max	Min	STDEV	Mean WEI-II	Max	Min	STDEV
Precipitation	S1	12	-0.0003	2.27	-3.72	0.98	0.01	3.18	-2.05	0.92
	S2	24	0.003	2.56	-3.14	1.01	0.02	3.73	-1.53	0.9
		12	-0.008	2.13	-4.15	0.96	0.01	3.21	-2.27	0.93
		24	0.0005	2.03	-2.85	1	0.01	2.75	-1.51	0.92
		12	-0.009	2.63	-4.73	0.97	0.02	4.25	-2.29	0.9
S3	24	0.001	2.52	-2.62	1	0.02	3.84	-1.35	0.9	
	12	-0.007	2.13	-3.86	0.968	0.01	3.24	0.01	0.95	
	24	-0.005	2.05	-2.67	0.968	0.009	3.32	-1.74	0.95	
	12	-0.02	2.006	-4.82	0.932	0.01	3.41	-2.87	0.955	
Runoff	S5	24	-0.01	1.91	-3.53	0.95	0.01	3.31	-2.03	0.95
		12	-0.004	1.72	-2.28	0.962	-0.01	2.07	-2.86	1.05
		24	-0.006	1.51	-2.3	0.957	-0.007	1.94	-2.22	1.02
		12	0.008	2.96	-1.55	1.02	-0.009	2.51	-2.74	1.03
	SH1	24	0.0005	2.08	-1.7	1	-0.01	2.003	-2.46	1.03
SH2	SH3	12	0.005	2.33	-2.01	1	0.005	2.82	-1.68	0.96
		24	-0.002	2.04	-2.47	0.97	0.005	2.81	-1.89	0.96
		12	-0.0003	3.81	-2.24	1.05	0.02	3.88	-2.14	0.91
		24	-0.004	3.6	-2.36	1.02	0.03	4.27	-1.62	0.89
	SH4	12	0.007	3.98	-1.44	1.13	0.02	3.2	-1.49	0.91
SH5	24	0.01	2.83	-1.45	1.09	0.01	2.47	-1.36	0.93	

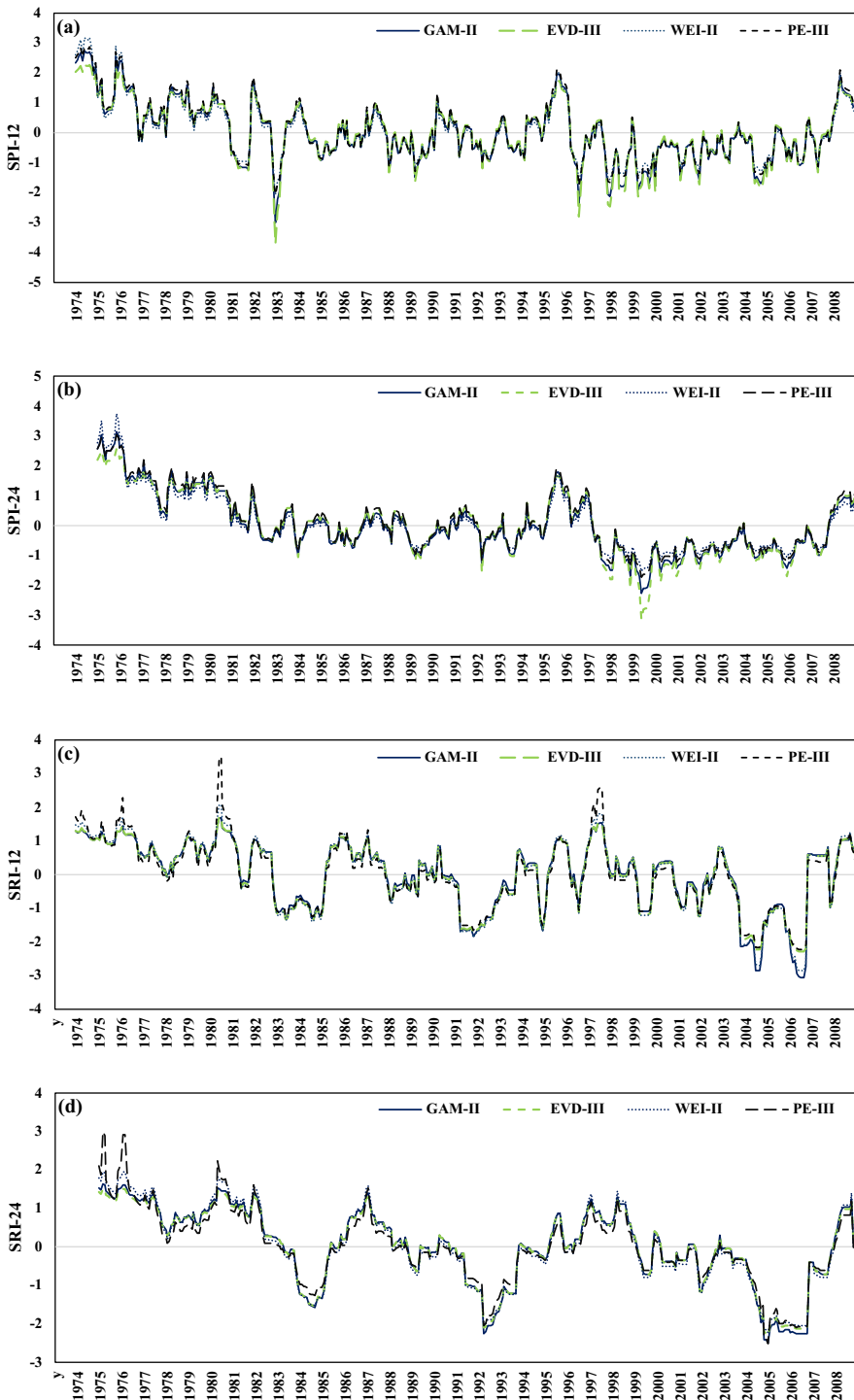


Fig. 3 Time series of SPI (a,b) and SRI (c,d) in the time scale of 12 at station S1 and SH1

Table 7 SPI/SRI estimation results of precipitation/runoff events in wet-dry periods when the distribution functions are different at stations S1 and SH1

Precipitation (mm)	Event	PE-III	GAM-II	EVD-III	WEI-II	Precipitation (mm)	Event	PE-III	GAM-II	EVD-III	WEI-II	WEI-I	
	SPI^c_{ij}	Wet period						Dry period					
39	$Y^{12}_{1975,6}$	2.81	2.67	2.23	3.10	9	$Y^{12}_{1983,12}$	-2.06	3.00	-3.72	-2.05		
38	$Y^{12}_{1976,6}$	2.69	2.54	2.15	2.89	11	$Y^{12}_{1997,7}$	-1.78	-2.36	-2.79	-1.69		
33	$Y^{12}_{1996,9}$	2.06	1.92	1.71	1.97	11	$Y^{12}_{1998,12}$	-1.65	-2.13	-2.46	-1.56		
33	$Y^{12}_{2009,4}$	2.08	1.94	1.72	2.00	13	$Y^{12}_{2005,9}$	-1.41	-1.69	-1.87	-1.29		
35	$Y^{24}_{1976,10}$	3.04	3.15	2.56	2.89	13	$Y^{24}_{2009,5}$	-1.73	-2.28	-3.14	-1.53		
Event	PE-III	GAM-II	EVD-III	WEI-II	Precipitation (mm)	Event	PE-III	GAM-II	EVD-III	WEI-II	Event		
Runoff (m^3/s)	SRI^c_{ij}	Wet period						Dry period					
4.13	$Y^{12}_{1981,5}$	3.44	1.68	1.71	2.06	0.13	$Y^{12}_{2005,8}$	-2.15	-2.84	-2.22	-2.69		
3.81	$Y^{12}_{1998,5}$	2.53	1.51	1.53	1.80	0.10	$Y^{12}_{2007,6}$	-2.22	-3.05	-2.28	-2.86		
3.37	$Y^{24}_{1975,12}$	3.00	1.62	1.51	1.94	0.42	$Y^{24}_{2005,12}$	-2.49	-2.54	-2.30	-2.22		

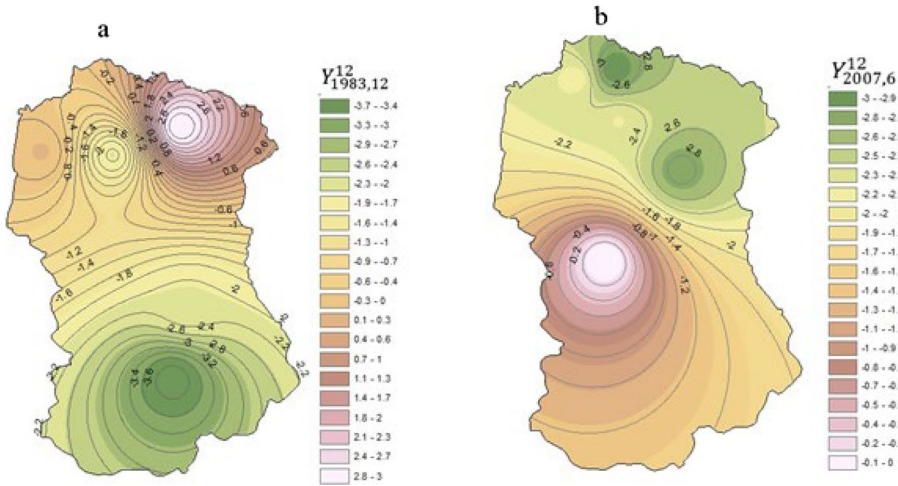


Fig. 4 Spatial drought mapping of $SPI^12_{1983,12}$ (a) and $SRI^12_{2007,6}$ (b) using EVD and Gamma III in the Mina Basin

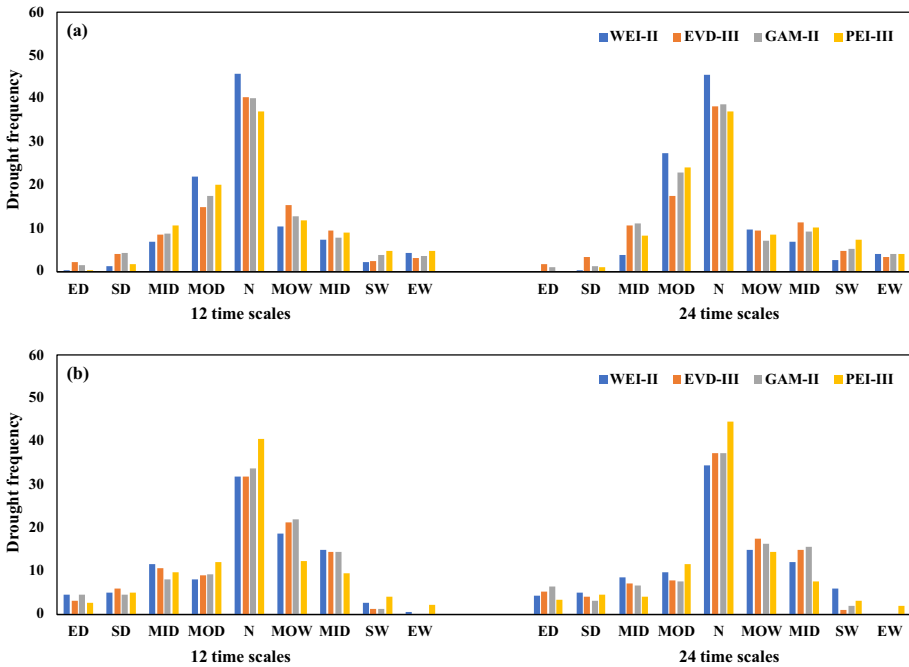


Fig. 5 Drought frequency in each category of wet/drought descriptive class (a) SPI and (b) SRI at 12 and 24-month time scales (*N*: normal; *EW*: extreme wet; *SW*: severe wet; *MW*: moderate wet; *MIW*: mild wet; *MOD*: moderate drought; *SD*: severe drought; *ED*: extreme drought) (Threshold value of each class presented in Table 3)

droughts in the study area fall within normal and mild drought classes, with percentages of normal conditions equal to 37% for the PEI-III, 40% for the GAM-II and the EVD-III and 47% for the WEI-II and percentages of mild drought conditions estimated to be 22%, 20%, 17% and 14% for the WEI-III, PEI-III, GAM-II and EVD-III functions, respectively. Similar results have been obtained for the SPI-24. In the two investigated scales, EVD-III and GAM-II functions compared to the other two functions have successfully estimated SD, ED drought events (Fig. 5a).

These results confirm past studies, such as Achite et al. (2023), evidencing that, in the Mediterranean regions of Algeria, due to the distribution of precipitation around the average, the condition of drought generally falls within the normal class.

As regards the SRI-12 (Fig. 5b), the PEI-III estimated more than 40% of the conditions to be normal, while the other functions estimated 32% on average. The 24-month time scales presents almost the same results. PEI-III and WEI-II functions have been considerably more successful in estimating historical drought events for both the time scales.

Generally, a higher frequency of hydrological droughts in the severe and extreme classes compared to meteorological droughts have been observed and this can be considered a consequence of climate change and anthropogenic activities (Aghakouchak et al. 2021; Zheng et al. 2023).

3.3 Uncertainty analysis

Based on the introduced methodology, for both the time scales, year and month, the values of SPI and SRI were calculated with 1000 production sampling and error values, bands and average. Table 8 shows some historical drought events in the investigated scales. The results of the 12-month historical drought with 9 mm rainfall, SPI estimated by the PEI-III is -2.06 , SPI estimated by bootstrap is -2.19 , estimation error (ARE) is 0.06, upper and lower band are -1.70 and -2.87 respectively, and the degree of uncertainty or band difference is 1.16. Considering the GAM-II, SPI is -3.00 , bootstrap SPI is -2.65 , estimation error is 0.11, upper and lower bands are -2.07 and -3.35

Table 8 The observed, estimated by bootstrap, simulation error, upper and lower bands of SPI and SRI in several historical drought events at station S1 and SH1

Value	SPI	OBS	EST	ARE	UB	LB	UN	OBS	EST	RE	UB	LB	UN
Y_{ij}^r		$Y_{1983,12}^{12}$						$Y_{2005,5}^{24}$					
PEI-III		-2.06	-2.19	0.06	-1.70	-2.87	1.16	-0.84	-0.097	0.15	-0.50	-1.55	1.04
GAM-II		-3.00	-2.65	0.11	-2.07	-3.35	1.27	-0.94	-0.99	0.05	-0.44	-1.65	1.21
EVD-III		-3.72	-2.86	0.23	-2.08	-4.07	1.99	-0.98	-0.95	0.03	-0.35	-1.68	1.33
WEI-II		-2.05	-2.03	0.008	-1.67	-2.44	0.76	-0.74	-0.93	0.24	-0.51	-1.40	0.88
SRI		$Y_{2007,6}^{12}$						$Y_{2005,12}^{24}$					
PEI-III		-2.22	-2.39	0.07	-1.70	-3.70	2.04	-2.51	-3.11	0.23	-1.94	-4.52	2.58
GAM-II		-3.05	-4.79	0.56	-3.79	-6.01	2.21	-2.49	-4.30	0.72	-3.08	-5.92	2.83
EVD-III		-2.28	-3.90	0.70	-2.99	-4.64	1.64	-2.30	-4.19	0.81	-3.25	-4.67	1.42
WEI-II		-2.86	-3.41	0.19	-2.93	-3.99	1.05	-2.22	-2.91	0.30	-2.33	-3.55	1.21

OBS SPI/SRI observed, **EST** SPI/SRI estimated, **AER** Absolute error ratio, **UB** Upper band, **LB** Lower band, **UN** Uncertainty

respectively, and the degree of uncertainty is 1.27. For the EVD-III, SPI is -3.72 , bootstrap SPI is -2.086 , estimation error is 0.23 , upper and lower bands are -2.08 and -4.07 , respectively, and the uncertainty level is 1.99 . Finally, as regards the WEI-II, SPI is -2.05 , bootstrap SPI is -2.03 , estimation error is 0.008 , upper and lower band are -1.67 and -2.44 , respectively, and uncertainty level is 0.76 . The changes in band values are shown in Fig. 6 (a1–a4). Based on the results, all the estimates for SPI are

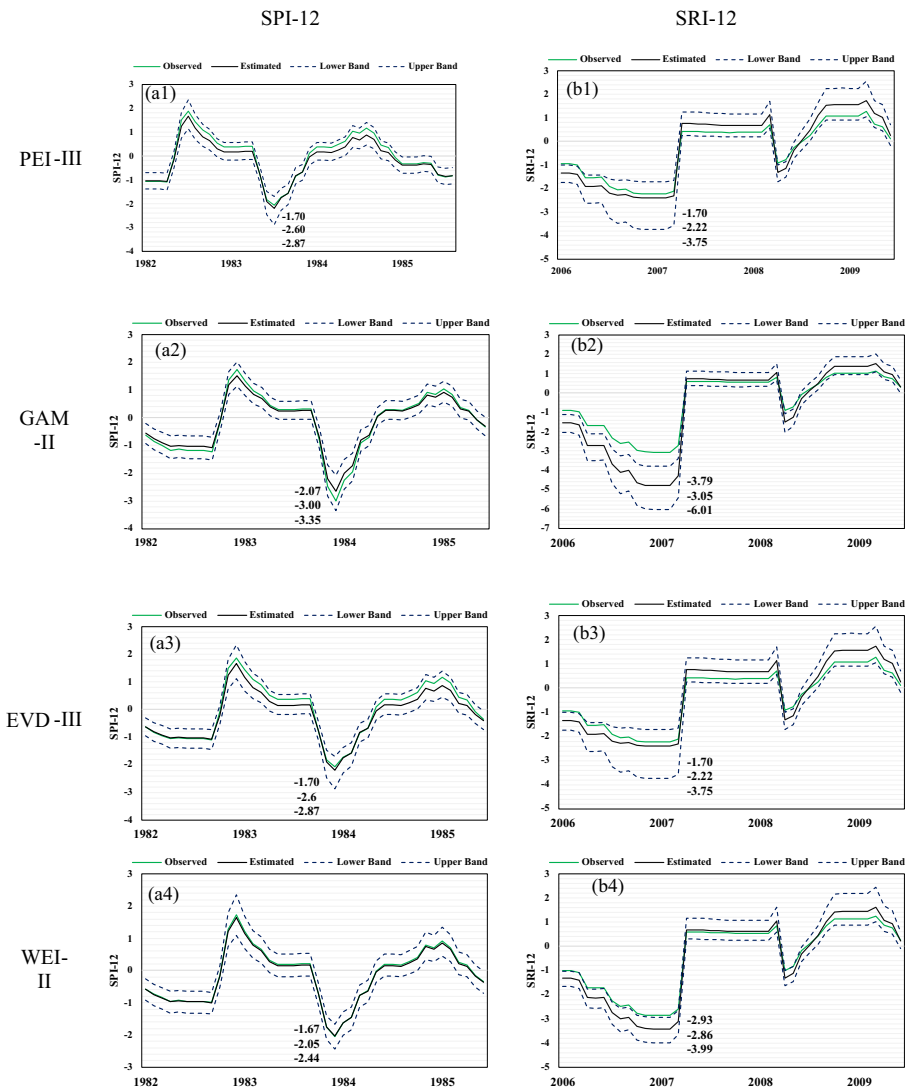


Fig. 6 Comparison of observed, estimated, upper and lower band $SPI_{1983,12}^{12}$ (a1–a4) and $SRI_{2007,6}^{12}$ (b1–b4) in station S1 and SH1 Zoning of upper band (a), lower band (b) and uncertainty (c) of $SPI_{1983,12}^{12}$ event in EVD-III function and zoning of $SRI_{2007,6}^{12}$ upper band (d), lower band (e) and uncertainty (f) in GAM-II are shown in Fig. 7 The interpolation is based on the kriging method

within the confidence range and the bootstrap estimated values are in good agreement with the observed values in all functions and are in the defined confidence band.

The same values were calculated for SRI historical events. For example, in the historical event of $Y_{2007,6}^{12}$ with a runoff of $0.1 \text{ m}^3/\text{s}$, the estimated SRI with the PEI-III is -2.22 , the SRI estimated by bootstrap is -2.39 , the estimated error is 0.07 , the upper and lower bands are -1.70 and -3.70 , and the amount of uncertainty or difference between the bands is 2.04 . For the GAM-II, with SRI is -3.05 , SPI estimated with bootstrap is -4.79 , estimated error is 0.56 , upper and lower band are -3.79 and -6.01 , respectively, and uncertainty level is 2.21 . In the EVD-III results, observed SRI is -2.28 , bootstrap SRI is -3.90 , estimated error is 0.70 , upper and lower bands are -2.99 and -4.64 , and the uncertainty is 1.64 . Considering the WEI-II, observed SRI is -2.86 , bootstrap SRI is -3.41 , estimated error is 0.19 , upper and lower band are -2.93 and -3.99 , respectively, and the uncertainty is 1.05 . The changes in upper and lower bands are shown in Fig. 6 (b1–b4). Based on the results, only for the PEI-III estimated and observed value fall within the uncertainty band, while for the other functions, although the SRI estimated is within the confidence band, the observed values are outside the band, and there is a great difference in the estimated and the observed event. In Fig. 6 (b1–b4), this discrepancy in historical event $Y_{2007,6}^{12}$ can be clearly understood. Most of the estimated values have maintained the observed trend, but in the minimum value of SRI that occurred (historical drought) on the mentioned date, the significance difference between observed and estimated is well evident.

As a result, considering the upper band (Fig. 7a) the central areas of the Mina Basin are the most vulnerable areas suffering from severe droughts ($\text{SPI} < -1.9$). These areas constitute 13% of the region surface, while more than 60% of the region in the northern and southern parts is under normal conditions ($\text{SPI} < -0.5$). In the lower band of the mentioned historical event, the central regions with an area of more than 15% are under severe and extreme droughts, while more than 50% of the region is under normal conditions. Therefore, from the comparison of the upper and lower bands, it emerges that the spatial pattern of drought does not change significantly among the maps, but in this example, the only factor affecting the size of the confidence interval is shown by the variability of the rainfall data of each station. Considering that the central parts have the highest intensity of drought, therefore the greatest distance between the upper and lower band is also in these places with an uncertainty of 2.2 , while the northern and southern parts have the lowest uncertainty.

Regarding the historical $\text{SRI}_{2007,6}^{12}$ event, the most vulnerable points in this event are the northern parts of the Mina basin, where the spatial pattern of the upper and lower band is similar, which indicates the highest variability of the runoff. The uncertainty of the estimates is also high in the northern parts.

Figure 8 shows the uncertainty and error rate for the different functions and time scales in the entire time range under investigation. The average uncertainties of SPI-12 (Fig. 8a) in the whole basin using PEI-III, GAM-II, EVD-III, WEI-II function are 0.8 , 0.742 , 1.14 and 0.742 , respectively, while the errors (Fig. 8b) are equal to 12.26 , 20.8 , 62.08 and 1.91 respectively. Therefore, on a 12-month scale in the case of SPI, WEI-II in the first degree and PEI-III in the second degree have the least uncertainty and error in meteorological stations. For the 24-month time scale, the average uncertainties of the SPI (Fig. 8c) in the whole basin using PEI-III, GAM-II, EVD-III, WEI-II function are 1.67 , 1.102 , 1.066 and 1.09 , respectively, with errors (Fig. 8d) equal to 11 , 38.2 , 55.04 and 26.2 respectively. Therefore, for this time scale, WEI-II and PEI-III functions have the least uncertainty and error. The comparison of uncertainty and error between the time scales showed that with the increase of the time scale and the decrease of the sample size, the amount of

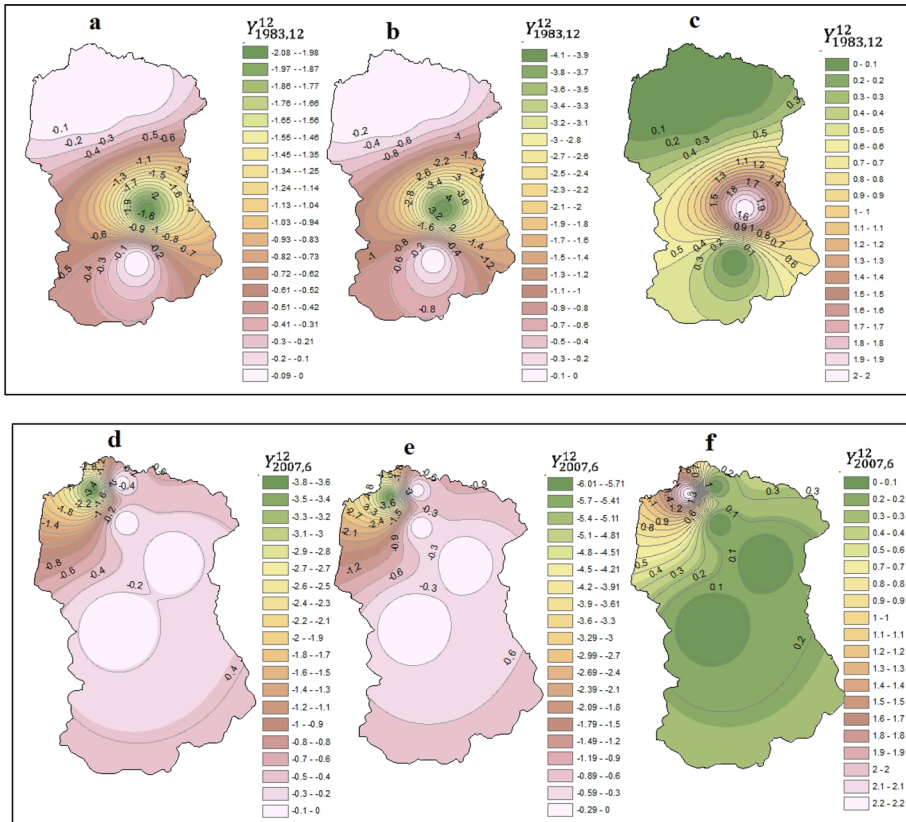


Fig. 7 Map of upper band (a), lower band (b) and uncertainty (c) $SPI_{1983,12}^{12}$ in in EVD-III and $SRI_{2007,6}^{12}$ zoning of upper band (d), lower band (e) and uncertainty (f) in the GAM -II

uncertainty and estimation error increases. In fact, on average, the amount of uncertainty and error in the SPI-12 are 0.85 and 24.24, respectively, while in the SPI-24 they are 1.106 and 32.61 respectively.

Researchers such as Guenang and Kanga (2014), Pieper et al. (2020) and Sherif et al. (2014) introduced WEI-II as the best function in SPI modeling while Zhang and Li (2020) believe that WEI-II has not been successful in estimating SPI in long and medium term periods and it is better to use it only for a short-term scale (1–3 months).

In the case of hydrological drought, the average uncertainties of SRI-12 (Fig. 8e) in the whole basin using PEI-III, GAM-II, EVD-III, WEI-II function are 1.064, 0.846, 0.828 and 0.872, respectively, with errors equal to 1.704, 1.542, 0.574 and 1.07 respectively (Fig. 8f). Therefore, on a 12-month scale in the case of SRI, EVD-III distribution has the lowest uncertainty and error in hydrometric stations. For the 24-month time scale, the average uncertainties of SRI-24 (Fig. 8g) in the whole basin using PEI-III, GAM-II, EVD-III, WEI-II function are 1.604, 1.34, 1.238 and 1.378 respectively, with errors equal to 1.73, 1.742, 1.57 and 1.66 respectively (Fig. 8h). Therefore, for this time scale, EVD-III has the least uncertainty. Regarding hydrological drought, increasing the time scale or reducing the sample size causes the uncertainty to increase from 0.90 to 1.36 and the error from 1.22 to

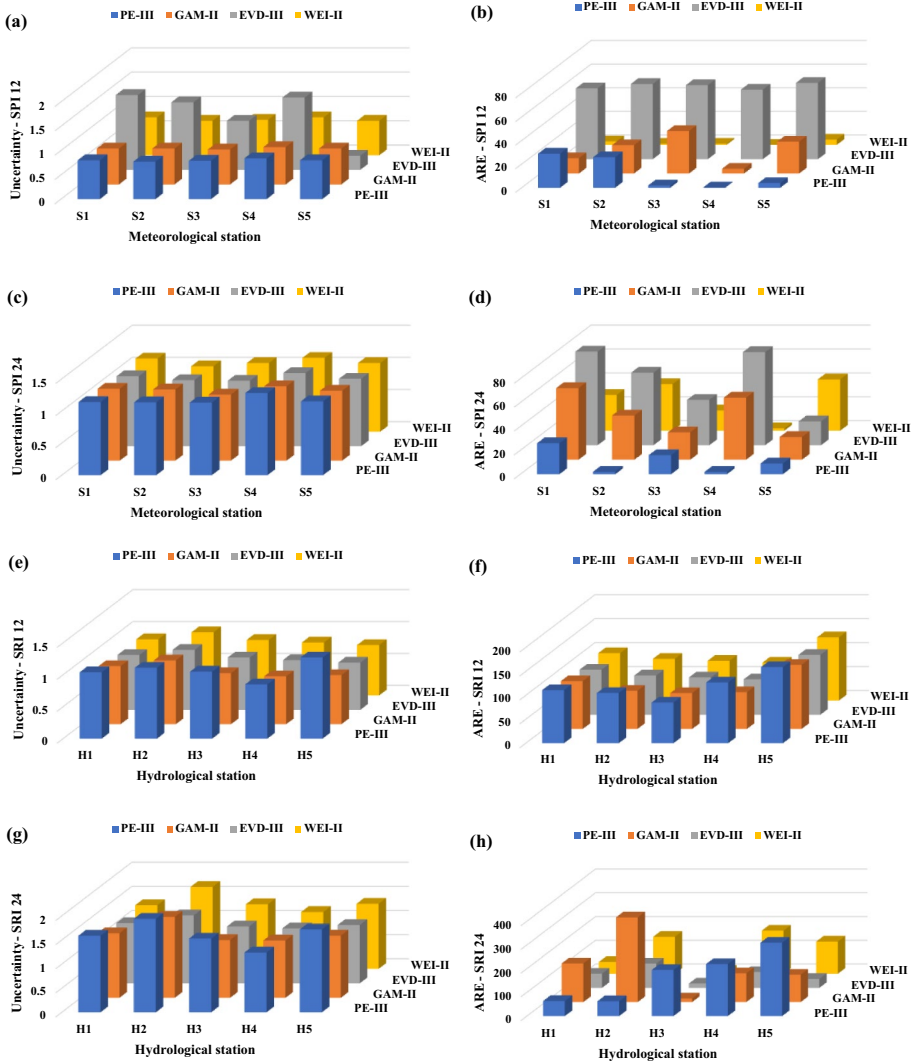


Fig. 8 Average of estimated error and uncertainty for the different functions and time scales. **a** and **c**: uncertainty of SPI 12 and 24; **b** and **d**: ARE of SPI 12 and 24; **e** and **g**: uncertainty of SRI 12 and 24; **f** and **h**: ARE of SRI 12 and 24

1.68. It is noteworthy that the uncertainty in SPI is lower and its error is higher compared to SRI. The greater the band difference, the lower the certainty and the greater the uncertainty (Vergni et al. 2015). The higher SPI error compared to SRI is due to the fact that this index reflects only precipitation data, since it does not include other factors, such as evaporation in the water balance. By contrast, the SRI reflects all hydrological processes influencing runoff; therefore, the error can be lower (Cerpa Reyes et al. 2022). Consequently, a longer period of time (more number of sampling) has less uncertainty, since the number of samples decreases as of the time scale increases, so the uncertainty bandwidth increases

as well. Perhaps one of the most important factors of higher ARE in SPI than in SRI is the greater precipitation variability compared to runoff.

Researchers such as Zhu et al. (2019), Vicente-Serrano et al. (2012), Shukla and Wood (2008) and Engeland et al. (2004) introduced the EDV-III function as the best distribution function in SRI modeling.

3.4 Comparison of the agreement between observed and estimated values in the severity of drought classes

To compare the agreement of the observed values with the bootstrap estimate in the assessment of the drought severity classes presented in Table 9, the weighted kappa statistic was used. The highest agreement between observed and estimated drought values in meteorological drought (almost perfect agreement) has been calculated in the WEI-II for both the SPI-12 and SPI-24. Then, the EVD-III and the GAM-II are placed in the class of substantial and almost perfect agreement, and the PE-II is in the class of substantial and moderate agreement.

The lowest agreement (slight and poor agreement) was observed for SRI-12 and SRI-24 by the EVD-III. Other functions have substantial and moderate agreement. In terms of the time scale, the lowest agreement in both indicators was seen in the 24-month time scale. Therefore, in a summary, it can be said that the WEI-II has the highest agreement in meteorological and hydrological drought in a time scale of 12 months (longer sample size).

3.5 Drought characteristics in observed and estimated values

Based on the presented methodology, drought characteristics including severity, duration, magnitude and peak were estimated for sample stations S1 and SH1. Figure 9, 10, 11 and 12 show the Max, Min and average characteristics for the observed and estimated values in different functions and time scales of SPI, SRI. It can be said that the characteristics of drought in the estimated values by bootstrap are far more than the observed values, especially in the 24-month scale in two indices.

Paired t-test was used to compare drought characteristics in observed and estimated characteristics. The statistical comparison of the mentioned characteristics is presented in Table 10. Based on the results, there is a significant difference between the severity and peak of SPI-12 estimated by the WEI-II and the PEI-III, while this significant difference does not emerge among any of the characteristics in different functions in SPI-24. An interesting result has been obtained considering the characteristics of drought in SRI-24 caused by the WEI-II. In fact, the results of the WEI-II have a significance difference with other distributions with the estimates in hydrological drought that are sometimes overestimated

Table 9 The weighted Cohen's kappa statistic between SPI/SRI observed and estimated

SPI/Kw	EVD-III	SA	GAM-II	SA	PE-III	SA	WEI-II	SA
SPI-12	0.77	S	0.89	AP	0.76	S	0.96	AP
SPI-24	0.64	S	0.75	S	0.58	M	0.84	AP
SRI-12	0.2	S	0.63	S	0.55	M	0.72	S
SRI-24	-0.06	P	0.6	M	0.49	M	0.66	S

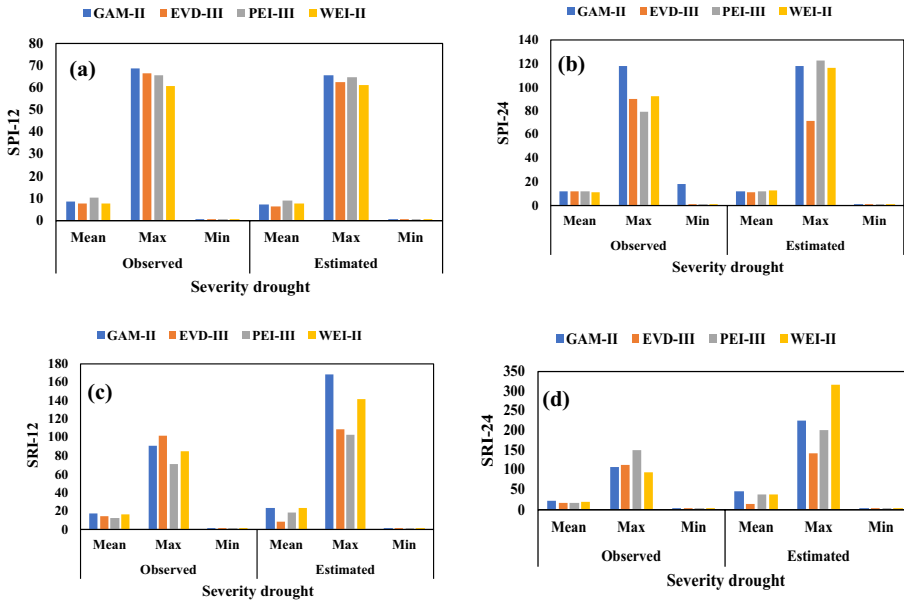


Fig. 9 Drought severity of SPI 12 (a), SPI 24 (b), SRI12 (c), SRI 24 (d) for different distribution functions

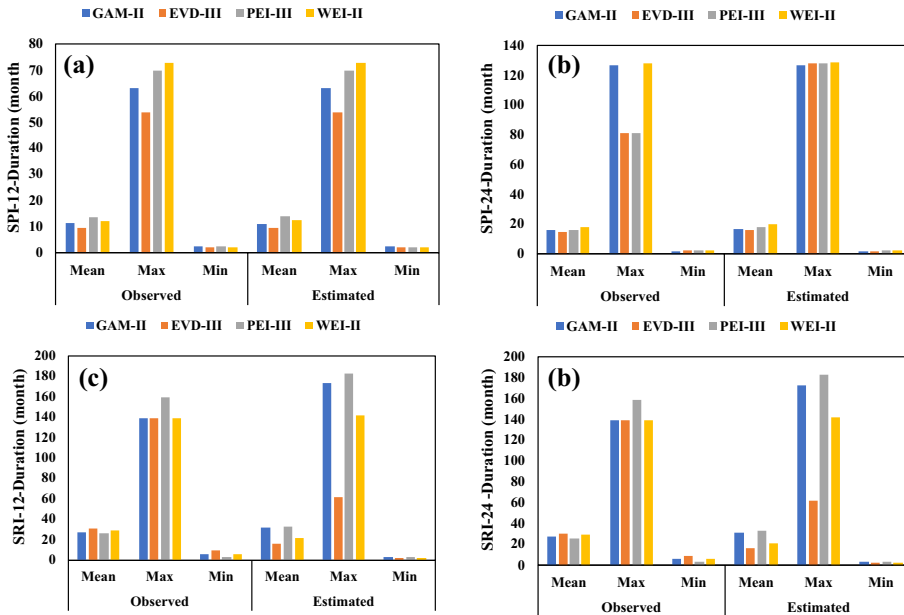


Fig. 10 Drought duration of SPI 12 (a), SPI 24 (b), SRI12 (c), SRI 24 (d); for different distribution functions

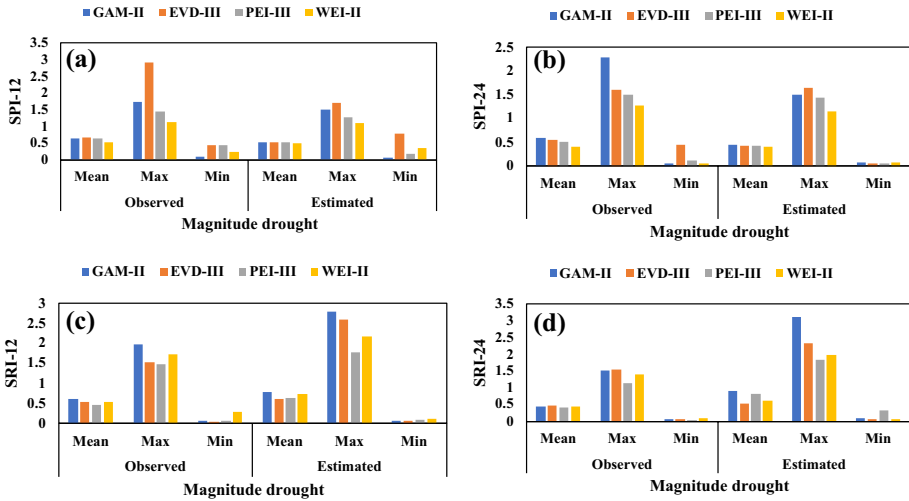


Fig. 11 Drought magnitude of SPI 12 (a), SPI 24 (b), SRI12 (c), SRI 24 (d); for different distribution functions

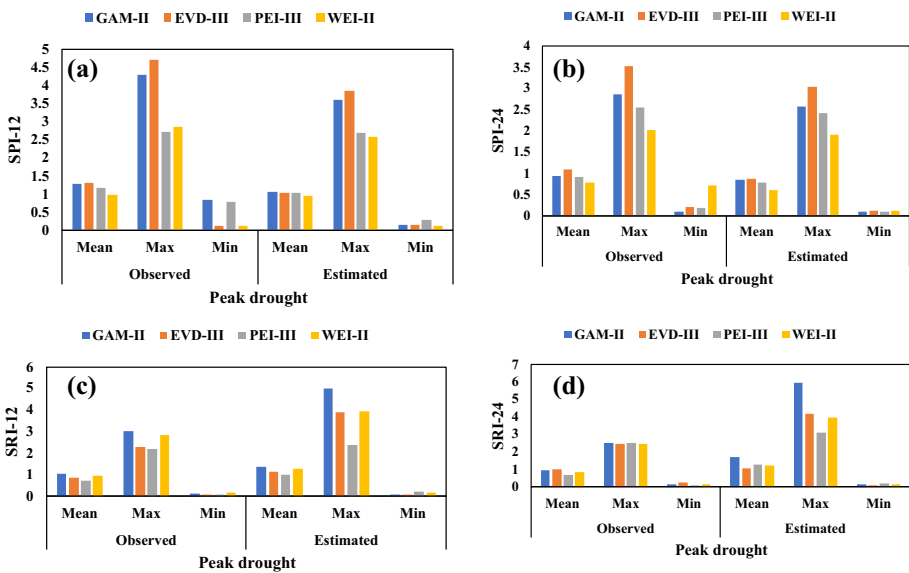


Fig. 12 Drought peak of SPI 12 (a), SPI 24 (b), SRI12 (c), SRI 24 (d); for different distribution functions

or underestimated compared to the other distribution functions. This situation is not evident in meteorological drought.

According to Vergni et al. (2017), as expected, the uncertainty increases when each record length decreases. Therefore, the main source of uncertainty is the length of the record, and the effects due to the time scale are insignificant. Because the uncertainties in time scale, record length and drought characteristics did not show significant difference.

Table 10 Comparison of drought characteristics in estimated and observed values of SPI and SRI

Characteristics	Distribution function				SPI24				
	SPI12		WEI-II		GAM-II		WEI-II		
Severity	GAM-II	-	0.045	0.295	-	0.757	0.914	0.914	
	EVD-III	-0.965	-1.205	0.739	-1.042	-1.226	-1.026	-1.026	
	PEI-III	0.045	-	4.459**	0.757	-	0.663	0.663	
	WEI-II	0.295	4.459**	-	0.914	-1.026	-	-	
Duration	GAM-II	-1.068	0.095	1.124	-0.846	0.641	-0.628	-0.628	
	EVD-III	0.095	-1.436	1.284	-	-1.126	-1.106	-1.106	
	PEI-III	1.124	-	1.142	0.641	-	-0.789	-0.789	
	WEI-II	1.124	1.284	-	-0.628	-1.016	-	-	
Magnitude	GAM-II	-0.812	0.293	0.675	-1.106	0.112	1.799	1.799	
	EVD-III	0.293	-0.15	-0.467	0.112	-1.738	-0.261	-0.261	
	PEI-III	0.675	-0.467	4.245**	1.799	-	1.018	1.018	
	WEI-II	-	4.245**	-	-	0.516	2.102	2.102	
Peak	GAM-II	-0.812	-0.015	0.467	-0.688	-0.868	0.334	0.334	
	EVD-III	0.293	-0.015	0.467	0.516	-	0.485	0.485	
	PEI-III	0.675	4.245**	-	2.102	0.334	-	-	
	WEI-II	-	4.245**	-	-	0.485	-	-	
SRI24									
Severity	GAM-II	-	2.244*	-	1.830	1.541	2.135	2.135	
	EVD-III	-0.56	2.450**	1.830	-	1.659	2.109	2.109	
	PEI-III	1.491	3.476**	1.541	1.659	-	2.470**	2.470**	
	WEI-II	2.244**	-	2.135	2.109	2.470**	-	-	
Duration	GAM-II	-	-1.22	-	-1.5	-1.00	1.5	1.5	
	EVD-III	1.322	-1.468	-1.5	-	-1.00	-1.464	-1.464	
	PEI-III	-1.624	-1.424	-1.00	-1.464	-	-1.10	-1.10	
	WEI-II	-1.22	1.46	1.50	-1.464	1.164	-	-	

Table 10 (continued)

	SRI12			SRI24					
Magnitude	GAM-II	-	-0.468	1.458	4.468**	-	1.134	1.134	3.444**
	EVD-III	-0.468	-	4.577**	1.458	1.195	1.209	1.209	3.07*
	PEI-III	1.458	1.487	-	10.05**	1.134	1.209	-	5.402**
	WEI-II	4.468**	4.577**	10.053**	-	3.444**	3.07**	5.402**	-
Peak	GAM-II	-	-0.646	2.171**	4.162**	-	1.252	1.966	33.211**
	EVD-III	-0.646	-	2.619**	4.950**	1.252	-	2.150	3.169**
	PEI-III	2.171**	2.619**	-	3.275**	1.966	2.150	-	4.765**
	WEI-II	4.162**	4.950**	3.275**	-	3.211**	3.169**	4.675**	-

**Significant at 99% level

The results of uncertainty of hydrological drought showed that two-parameter distributions (WEI-II, GAM-II) produce shorter confidence intervals than three-parameter distributions (EVD-III, PE_III). However, due to the poorer fit of two-parameter distributions to runoff values, estimates from these two-parameter distributions may provide less reliable runoff probability. Therefore, drought characteristics will be significantly different from the values of two-parameter distribution functions.

Regardless of the type of distribution function and the number of parameters, the estimated SRI related to extreme values of runoff is always associated with an uncertainty. This uncertainty is due to the variability of the hypothetical distribution function that is used and this situation occurs when the data (runoff) approaches the tails of this hypothetical distribution function.

As regards the meteorological drought uncertainty, the WEI-II distribution function had the lowest uncertainty, and its drought characteristics showed a significant difference with the PEI-III. According to Zamani and Bazarfashan (2020), in the regions with high fluctuations of precipitation regimes, the standard deviation is high; therefore, the coefficient of variation of precipitation (the ratio of standard deviation to the average precipitation) is high, causing an increase in kurtosis and light tail. This situation indicates the high frequency of irregular rainfall events throughout the year in Mediterranean regions. In this case, the WEI-II distribution function will be the best estimate of drought (Table 10).

4 Conclusion

Drought investigation is now one of the most important challenges, especially in arid and semi-arid regions. SPI and SRI are simple and commonly used indicators for meteorology and hydrology drought. Despite their simplicity, both indicators are based on the statistical distribution of precipitation and runoff time series. The properties of these time series can depend on the estimates of parameters in statistical distributions, ultimately affecting the uncertainty of drought analysis. This is particularly important in the context of spatial and temporal drought analysis and projections.

The objectives of this work were to analyze the uncertainty of meteorological and hydrological droughts based on SPI and SRI in the wadi Mina basin in northwest Algeria. The following distributions of precipitation and runoff time series were considered: Gamma (GA), Weibull (WEI), Extreme value (EVD), and Pearson (PE). Bootstrap methods were used to generate samples of data, and subsequently, the uncertainty of both drought indicators was assessed.

The results show that all considered distributions were acceptable fits for the time series, and the time scale of the data was not significantly related to the goodness of fit. Moreover, there was no apparent relationship between the rejection cases and the scale and position of the regional stations or the investigated variable. The lack of significant differences between time series for a particular distribution caused the averages estimated in SPI to fall within the same descriptive class. The most severe meteorological droughts were observed for the PE-III function and the EVD-III function. In the case of hydrological drought, the most severe drought was estimated by the WEI-II and the GAM-II. The type of periods (dry or wet) depends on the type of distribution of the data. In general, for meteorological drought, the EVD-III represents the most severe drought, and the WEI-II has estimated values of lower intensities. Regarding hydrological drought, all events are rated as the most severe for the EVD-III.

In the uncertainty analysis, most of the observed SPI values fell within the confidence range for all distributions, both for the SPI and the SRI. Only in the case of the SRI, results from the PEI-III were above the true value in the bootstrap band. Based on the weighted Kappa statistics, the highest agreement between observed and estimated values for both kinds of drought occurred with the WEI-II at SPI 12 and SPI 24. Following this function, the EVD-III and the GAM-II showed substantial and almost perfect agreement, while the PEI-III fell into the category of substantial and moderate agreement.

The results of the results, WEI-II has the lowest estimation error and uncertainty in meteorological drought in the two investigated time scales, but in hydrological drought it is related to EVD-III. Investigating the use of the two mentioned functions for drought monitoring in two medium-term and long-term time scales is recommended.

These results are important from a methodological perspective because they highlight the necessity of including uncertainty in drought analysis, especially now when future climate projections are subject to strong uncertainty. It is also crucial to select the statistical distribution for calculating SPI and SRI appropriately, especially for longer time-periods.

Considering the temporal distribution of precipitation and its effect on runoff in Mediterranean regions, the results of this study can help to develop a meteorological/hydrological drought warning and monitoring system in similar regions.

Acknowledgements We thank the National Agency of the Water Resources (ANRH) for the collected data and the General Directorate of Scientific Research and Technological Development of Algeria (DGRSDT).

Author contributions All authors contributed to the study's conception and design. MA, OB: Collecting data, preparing and calculation, editing and reviewing manuscripts; OB, ZP and FP: Data analysis, plotting, and manuscript preparation; TC: Writing introduction; AW: Writing conclusion. All authors read and approved the final manuscript.

Funding The authors declare that no funds, grants, or other support, were received during the preparation of this manuscript.

Data availability Not applicable.

Declarations

Conflict of interest The authors declare that they have no known competing financial interests or personal relationships that could have appeared to influence the work reported in this paper.

Ethical approval We confirm that this article is original research and has not been published previously in any journal in any language.

Consent to participate All the authors read and approved the final version of the manuscript.

Consent to publish The authors confirm that the work described has not been published before, and it is not under consideration for publication elsewhere.

References

- Achite M, Ouillon S (2007) Suspended sediment transport in a semiarid watershed, Wadi Abd, Algeria (1973–1995). *J Hydrol* 343(3–4):187–202
- Achite M, Simsek O, Adarsh S, Hartani T, Caloiero T (2023) Assessment and monitoring of meteorological and hydrological drought in semiarid regions: the Wadi Ouahrane basin case study (Algeria). *Phys Chem Earth* 130:103386

- AghaKouchak A, Mirchi A, Madani K, Di Baldassarre G, Nazemi A, Alborzi A, Wanders N (2021) Anthropogenic drought: definition, challenges, and opportunities. *Rev Geophys* 59(2):1–23
- Angelidis P, Maris F, Kotsovinos N, Hrisanthou V (2012) Computation of drought index SPI with alternative distribution functions. *Water Resour Manag* 26:2453–2473
- Azhdari Z, Bazrafshan O, Zamani H, Shekari M, Singh VP (2021) Hydro-meteorological drought risk assessment using linear and nonlinear multivariate methods. *Phys Chem Earth Parts a/b/c* 123:103046
- Bazrafshan O, Mahmoudzadeh F, Bazarafshan J (2015) Evaluation of drought changes based on standardized precipitation index and standardized evapotranspiration index in southern coasts of Iran. *Sci Res J Desert Manag*. <https://doi.org/10.22034/JDMAL.2017.24662>
- Bazrafshan O, Zamani H, Shekari M (2020) A copula-based index for drought analysis in arid and semi-arid regions of Iran. *Nat Res Model* 33(1):e12237
- Blain GC (2012) Revisiting the probabilistic definition of drought: strengths, limitations and an agrometeorological adaptation. *Bragantia Campinas* 71(1):132–141
- Bordi I, Fraedrich K, Jiang J-M, Sutera A (2004) Spatio-temporal variability of dry and wet periods in eastern China. *Theor Appl Climatol* 79:81–91
- Bordi I, Fraedrich K, Sutera A (2009) Observed drought and wetness trends in Europe: an update. *Hydrol Earth Syst Sci* 13:1519–1530
- Buttafuoco G, Caloiero T (2014) Drought events at different timescales in southern Italy (Calabria). *J Maps* 10:529–537
- Buttafuoco G, Caloiero T, Ricca N, Guagliardi I (2018) Assessment of drought and its uncertainty in a southern Italy area (Calabria region). *Measurement* 113:205–210
- Cerpa Reyes LJ, Ávila Rangel H, Herazo LC (2022) Adjustment of the standardized precipitation index (SPI) for the evaluation of drought in the Arroyo Pechelín basin, Colombia, under zero monthly precipitation conditions. *Atmosphere* 13(2):236. <https://doi.org/10.3390/atmos13020236>
- Cohen J (1968) Weighted kappa: Nominal scale agreement provision for scaled disagreement or partial credit. *Psychol Bulletin* 70(4):213
- Dixon PM (2006) Bootstrap resampling. *Encyclopedia Environmetrics*
- Engeland K, Hisdal H, Frigessi A (2004) Practical extreme value modelling of hydrological floods and droughts: a case study. *Extremes* 7:5–30
- Ghasemnejad F, Fazeli M, Bazarafshan O, Parveen Nia M (2018) Uncertainty analysis of hydrological drought characteristics using Latin hypercube (case study: Minab Dam watershed). *Pasture and Watershed Sci-Res J* 72(2):527–542. <https://doi.org/10.22059/jrwm.2019.276424.1356>
- Ghasemnejad F, Fazeli M, Bazarafshan O, Parvinnia M, Singh VP (2022) Uncertainty analysis of hydrological drought due to record length, time scale, and probability distribution functions using Monte Carlo simulation method. *Atmosphere* 13(9):1390
- Guenang GM, Kamga FM (2014) Computation of the standardized precipitation index (SPI) and its use to assess drought occurrences in Cameroon over recent decades. *J Appl Meteorol Climat* 53(10):2310–2324
- Guttman NB (1994) On the sensitivity of sample L moments to sample size. *J Clim* 7(6):1026–1029
- Guttman NB (1999) Accepting the standardized precipitation index: a calculation algorithm. *J Am Water Res* 35:311–322
- Guttman NB (1999) Accepting the standardized precipitation index: a calculation algorithm. *J Am Water Res* 35:311–322
- Hayes MJ, Svoboda MD, Wilhite DA, Vanyarkho OV (1999) Monitoring the 1996 drought using the standardized precipitation index. *Bull Am Meteorol Soc* 80:429–438
- Hu YM, Liang ZM, Liu YW, Wang J, Yao L, Ning Y (2015) Uncertainty analysis of SPI calculation and drought assessment based on the application of bootstrap. *Int J Climatol* 35:1847–1857
- Khatun J, Ramkissoon K, Giddings MC (2007) Fragmentation characteristics of collision-induced dissociation in MALDI TOF/TOF mass spectrometry. *Anal Chem* 79(8):3032–3040
- Landis JR, Koch GG (1977) The measurement of observer agreement for categorical data. *Biometrics* 159–174
- Lloyd-Hughes B, Saunders MA (2002) A drought climatology for Europe. *Int J Climatol* 22:1571–1592
- McKee TB, Doseken NJ, Kleist J, (1993) The Relationship of Drought Frequency and Duration to Time Scales In: *proc. 8th Conf. On Applied Climatology*, American Meteorological Society, Massachusetts pp 179–184.
- McKee TB, Doesken NJ and Kleist J (1993). The relationship of drought frequency and duration to time scales. Pp 179–184. In *Proceedings of the 8th Conference of Applied Climatology*. 17–22, Anaheim, California.

- Mishra AK, Desai VR (2005) Drought forecasting using stochastic models. *Stoch Environ Res Risk Assess* 19:326–339
- Naumann G, Barbosa P, Carrao H, Singleton A, Vogt J (2012) Monitoring drought conditions and their uncertainties in Africa using TRMM data. *J Appl Meteorol Clim* 51:1867–1874
- Pieper P, Düsterhus A, Baehr J (2020) A universal Standardized Precipitation Index candidate distribution function for observations and simulations. *Hydrol Earth Syst Sci* 24(9):4541–4565
- Sherif M, Almulla M, Shetty A, Chowdhury RK (2014) Analysis of rainfall, PMP and drought in the United Arab Emirates. *Int J Climatol* 34(4):1318–1328
- Shukla S and Wood AW (2008) Use of a standardized runoff index for characterizing hydrologic drought. *Geophysical research letters*. 35(2)
- Shukla S, Wood AW (2008) Use of a standardized runoff index for characterizing hydrologic drought. *Geophys Res Lett* 35:L02405
- Spinoni J, Naumann G, Carrao H, Barbosa P, Vogt J (2014) World drought frequency, duration, and severity for 1951–2010. *Int J Climatol* 34:2792–2804
- Stagge JH, Tallaksen LM, Gudmundsson L, Van Loon AF, Stahl K (2015) Candidate distributions for climatological drought indices (SPI and SPEI). *Int J Climatol* 35(13):4027–4040
- Tramblay Y, Koutroulis A, Samaniego L, Vicente-Serrano SM, Volaire F, Boone A, Le Page M, Llasat MC, Albergel C, Burak S et al (2020) Challenges for drought assessment in the Mediterranean region under future climate scenarios. *Earth-Sci Rev* 210:103348
- Verdonck FA, Jaworska J, Thas O, Vanrolleghem PA (2001) Determining environmental standards using bootstrapping, Bayesian and maximum likelihood techniques: a comparative study. *Anal Chim Acta* 446(1–2):427–436
- Vergni L, Di Lena B, Todisco F, Mannocchi F (2017) Uncertainty in drought monitoring by the standardized precipitation index: the case study of the Abruzzo region (central Italy). *Theor Appl Climatol* 128(1–2):13–26
- Vicente-Serrano SM, Beguería S, López-Moreno JI (2010) A multiscalar drought index sensitive to global warming: the standardized precipitation evapotranspiration index. *J Clim* 23:1696–1718
- Vicente-Serrano SM, López-Moreno JI, Beguería S, Lorenzo-Lacruz J, Azorin-Molina C, Morán-Tejada E (2012) Accurate computation of a streamflow drought index. *J Hydrol Eng* 17(2):318–332
- Wu H, Hayes MJ, Wilhite DA, Svoboda MD (2005) The effect of the length of record on the standardized precipitation index calculation. *Int J Climatol: A J Royal Meteorol Soc* 25(4):505–520
- Wu H, Svoboda MD, Hayes MJ, Wilhite DA, Wen F (2007) Appropriate application of the standardised precipitation index in arid locations and dry seasons. *Int J Climatol* 27:65–79
- Zamani H, Bazrafshan O (2020) Modeling monthly rainfall data using zero-adjusted models in the semi-arid, arid and extra-arid regions. *Meteorol Atmos Phys* 132(2):239–253
- Zhang Y, Li Z (2020) Uncertainty analysis of standardized precipitation index due to the effects of probability distributions and parameter errors. *Front Earth Sci* 8:76
- Zheng J, Zhou Z, Liu J, Yan Z, Xu CY, Jiang Y, Wang H (2023) A novel framework for investigating the mechanisms of climate change and anthropogenic activities on the evolution of hydrological drought. *Sci Total Environ* 900:165685
- Zhu S, Xu Z, Luo X, Wang C, Zhang H (2019) Quantifying the contributions of climate change and human activities to drought extremes, using an improved evaluation framework. *Water Res Manag* 33:5051–5065

Publisher's Note Springer Nature remains neutral with regard to jurisdictional claims in published maps and institutional affiliations.

Springer Nature or its licensor (e.g. a society or other partner) holds exclusive rights to this article under a publishing agreement with the author(s) or other rightsholder(s); author self-archiving of the accepted manuscript version of this article is solely governed by the terms of such publishing agreement and applicable law.

Authors and Affiliations

Mohammad Achite^{1,2} · Ommolbanin Bazrafshan³  · Zohreh Pakdaman⁴ · Andrzej Wałęga⁵ · Fateme Pourhaghverdi³ · Tommaso Caloiero⁶

✉ Ommolbanin Bazrafshan
o.bazrafshan@hormozgan.ac.ir

Mohammad Achite
m.achite@univ-chlef.dz

Zohreh Pakdaman
zpakdaman@hormozgan.ac.ir

Andrzej Wałęga
andrzej.walega@urk.edu.pl

Fateme Pourhaghverdi
fpourhaghverdi@hormozgan.ac.ir

Tommaso Caloiero
tommaso.caloiero@cnr.it

¹ Laboratory of Water and Environment, Faculty of Nature and Life Sciences, Hassiba Benbouali University of Chlef, 02180 Chlef, Algeria

² Georesources, Environment and Natural Risks Laboratory, University of Oran, 2 Mohamed Ben Ahmed, P.Box 1015 El M'naouer, 31000 Oran, Algeria

³ Department of Natural Resources Engineering, Faculty of Agriculture and Natural Resources Engineering, University of Hormozgan, Bandar-Abbas 7916193145, Iran

⁴ Department of Statistics, Faculty of Science, University of Hormozgan, Bandar-Abbas 7916193145, Iran

⁵ Department of Sanitary Engineering and Water Management, University of Agriculture in Krakow, Mickiewicza 24/28 Street, 30-059, Krakow, Poland

⁶ National Research Council of Italy, Research Institute for Geo-Hydrological Protection (CNR-IRPI), Rende, Italy